DEPARTMENT OF MANAGEMENT AND ENGINEERING

Constitutive modelling of the nickel base superalloy IN718; a preparatory study

Master Thesis carried out at Division of Solid Mechanics
Linköpings University
November 2008

David Gustafsson

LIU-IEI-TEK-A--08/00489--SE

Linköping University
INSTITUTE OF TECHNOLOGY

**Institute of Technology, Dept. of Management and Engineering,
SE-581 83 Linköping, Sweden**

Framläggningsdatum Presentation date 2008-11-28 **Publiceringsdatum** Publication date 2008-11-28	**Avdelning, institution** Division, department Division of Solid Mechanics Dept. of Management and Engineering SE-581 83 LINKÖPING INSTITUTE OF TECHNOLOGY LINKÖPINGS UNIVERSITET

Språk Language Svenska/Swedish X Engelska/English	**Rapporttyp** Report category Licentiatavhandling X Examensarbete C-uppsats D-uppsats Övrig rapport	**ISBN:** **ISRN:** LIU-IEI-TEK-A--08/00489--SE **Serietitel:** Title of series **Serienummer/ISSN:** Number of series

URL för elektronisk version
URL for electronic version
[illegible]

Titel Title	Constitutive modelling of the nickel base superalloy IN718, a preparatory study
Författare Author	David Gustafsson

Sammanfattning
Abstract

One of the limiting factors in gas turbine design is the allowable metal temperatures and loads in critical components. Specially designed superalloys are used when the conditions are most severe. One of these superalloys is Inconel 718. To be able to design components for higher temperature and higher loads, an accurate understanding and computational model of the material is needed. In this thesis the deformation mechanisms of Inconel 718 have been investigated and a theoretical basis for modelling in a large deformation context has been established. Finally a viscoplastic nonlinear kinematic hardening material model with an Armstrong-Frederick backstress evolution law has been implemented as a first step in describing the constitutive behaviour of the material Inconel 718.

Nyckelord: material model, superalloy, cyclic behaviour, Armstrong-Fredrick, LS-DYNA, FORTRAN
Keyword

Abstract

One of the limiting factors in gas turbine design is the allowable metal temperatures and loads in critical components. Specially designed superalloys are used when the conditions are most severe. One of these superalloys is Inconel 718.

To be able to design components for higher temperature and higher loads, an accurate understanding and computational model of the material is needed. In this thesis the deformation mechanisms of Inconel 718 have been investigated and a theoretical basis for modelling in a large deformation context has been established.

Finally a viscoplastic nonlinear kinematic hardening material model with an Armstrong-Frederick backstress evolution law has been implemented as a first step in describing the constitutive behaviour of the material Inconel 718.

Preface

The work presented here is a master thesis performed at the Division of Solid Mechanics at Linköping University from summer to winter 2008. The work has been carried out by funding from the research program TURBOKRAFT, see www.turbokraft.se.

I would like to thank my two supervisors, professor Kjell Simonsson and professor Sören Sjöström, for all the invaluable help and guidance during the work of this master thesis. I would like to thank all the Ph.D. student colleagues at the division, especially Daniel Leidermark and David Lönn for all their help. I would like to thank the people at SIEMENS in Finspång, especially Tech. Lic. Per Ahlmroth, Dr. Johan Moverare and Dr. Magnus Hasselqvist for helping me to understand the difficulties in deformation mechanisms and modelling of Inconel 718.

A great appreciation should also be given to my family, girlfriend and friends for all their support.

David Gustafsson

Linköping, November 2008

Nomenclature

Variable	Description
$\boldsymbol{B}$	Backstress tensor
$\boldsymbol{b}$	Internal state variable
$\boldsymbol{C}^e$	The elastic right Cauchy-Green strain tensor
C_l	Elastic tangent stiffness tensor
$C_1,\ C_2$	Material constants
$\boldsymbol{D}$	Rate of deformation tensor
dev$\boldsymbol{B}$	Deviatoric part of backstress tensor
dev$\boldsymbol{\mathfrak{M}}$	Deviatoric part of Mandel stress tensor
$\boldsymbol{E}^e$	Elastic Green-Lagrange strain tensor
E	Modulus of elasticity
e	Internal energy
e_{el}	Elastic part of the internal energy
e_{pl}	Plastic part of the internal energy
$\boldsymbol{F}$	Total deformation gradient
$\boldsymbol{F}^e$	Elastic deformation gradient
$\boldsymbol{F}^p$	Plastic deformation gradient
G	Shear modulus
$\boldsymbol{I}$	Unit tensor
K	Bulk modulus
$\boldsymbol{L}$	Velocity gradient
m	Material constant
R_ϵ	Strain ratio
$\boldsymbol{S}$	2:nd Piola-Kirchhoff stress tensor
$\boldsymbol{W}$	Spin tensor
Δt	Time step
$\mathcal{J}$	Jacobian determinant
λ	Lamé constant
$\dot{\lambda}$	Plastic multiplier
λ_0	Material constant
μ	Lamé constant

Variable	Description
$\boldsymbol{\mathcal{M}}$	Mandel stress tensor
$\mathcal{P}^{int}$	Internal power
ρ	Density
$\boldsymbol{\sigma}$	Cauchy stress tensor
σ_e	Effective stress according to von Mises
σ_Y	Yield stress
$\boldsymbol{\tau}$	Kirchhoff stress tensor
$\mathcal{D}$	Thermodynamic dissipation
$\boldsymbol{\phi}$	Plastic lattice rotation
Ω	Current configuration
$\bar{\Omega}$	Intermediate configuration
$\bar{\Omega}_{iso}$	Isoclinic intermediate configuration
Ω_0	Reference configuration

Contents

List of Figures

List of Tables

1 Background

In gas turbines it is important to design for as high gas temperatures as possible in order to attain a high thermal efficiency. The high-temperature load carrying ability of significant components is therefore one of the most important factors that set the limit in gas turbine design. Even though particular high temperature resistant superalloys are used, hot components are usually designed to run near their temperature and load limit. Uncertainties in models and methods used for fatigue life prediction under these circumstances are very problematic. Usual ways to handle the situation are to:

- Reduce the temperatures or loads to attain a better safety margin meaning conservative design and lower thermal efficiency than would otherwise be possible.
- Prescribe shorter inspection and component exchange intervals meaning cost increase and loss in engine availability.

Among the most important questions in gas turbine design is therefore how to predict the life of such components. The usual load case for these components is a start/stop low-cycle fatigue cycle combined with a hold time at high temperature, where this hold time load is high enough to cause time dependent effects such as creep deformation. Another complicating fact is that the mechanical properties degrade during long time exposure to high temperature and cyclic loads by e.g. microstructural changes and oxidation, thus reducing the fatigue resistance of the material.

1.1 Ph.D project, Influence of high temperature hold times on the fatigue life of nickel-based superalloys

The Ph.D project concerns the question of how thermo-mechanical cycling in combination with hold times at high temperatures governs the fatigue behavior, i.e. the initiation and propagation of fatigue cracks, of gas turbine materials. By considering the effect of the cyclic loading, time-dependent inelastic deformations (creep) and environmental effects (oxidation etc.), enhanced models for life time predictions are to be set up, which are not only capable of describing the observed fatigue behavior, but also simple enough to be used in real industrial applications. The knowledge gained in the project will not only be directly usable in the design of more efficient gas turbines of today, but will also be important for the long run development towards

an increased use of renewable fuels. This master thesis is a first step in the Ph.D project.

1.2 Gas turbines

The gas turbine is used for jet propulsion and electricity generation. The efficiency of a gas turbine is highly temperature dependent. The gas turbine extracts energy from a flow of hot gases. It has three major components: a compressor, a combustor and a turbine; see Figure 1. Air is drawn from the inlet into the compressor where it is pressurized in several compressor steps. Some of the air is lead into the gas turbine's cooling system while the main part of the air is lead to the combustor where the combustion of fuel heats the air. The hot gas is then lead into the turbine where the energy of the hot gas is converted into rotation of the turbine. The turbine shaft drives the compressor and, in case of a stationary electricity-generating gas turbine, a generator as well [1]. In the last stage the air is allowed to expand converting static pressure into dynamic pressure further increasing the velocity of the air. In the stationary gas turbines there is a power turbine generating electricity and in case of jet engines the higher air velocity means extra thrust [2].

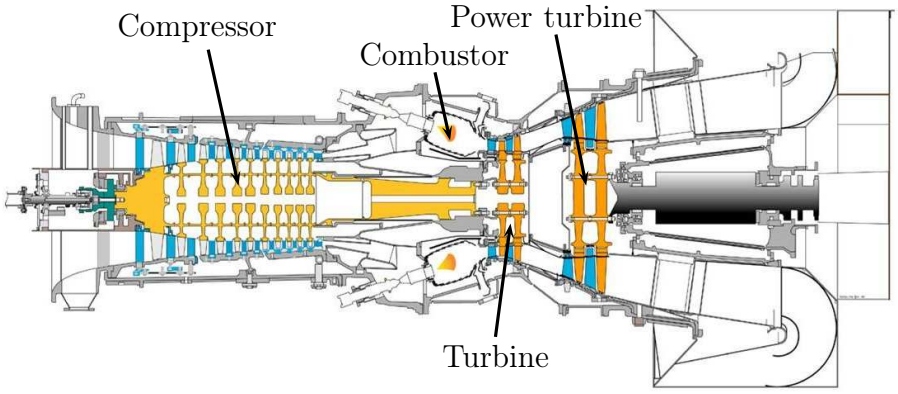

Figure 1: The interior of a stationary gas turbine, with permission from SIEMENS

As discussed earlier it is of interest to raise the turbine temperature as much as possible. One major factor limiting this is the allowed metal temperatures of the components in the turbine. To be able to design components for higher temperatures it is of importance to understand the material behavior and to be able to model it in a correct and usable way [3].

2 Nickel base superalloys

The nickel-based superalloys were created in the 1940's primarily for gas turbine applications because of their long-time strength and toughness at high temperatures. The early superalloys contained 80%Ni and 20%Cr [3]. Since then a huge number of alloying elements such as titanium, aluminium, tungsten, etc. has been added to enhance their mechanical properties. The modern nickel-base superalloy has a γ matrix that has a face-centered cubic (FCC)[1] crystal structure as well as dispersed coherent γ' particles. Some nickel-base superalloys containing a lot of Fe usually have dispersed coherent γ'' [2] particles as well as γ' particles. The precipitates make up as much as 50% of the volume of the material, and act as a hard strengthening phase in the ductile γ matrix [3].

There are some main reasons for the good temperature behaviour of nickel. The FCC structure of nickel is both ductile and tough. Nickel is also stable in its FCC structure when heated from room temperature up to its melting point. Nickel has a high activation energy for self-diffusion which makes it resistant to creep deformation. Other materials which display this crystal structure and behaviour are dense and/or very expensive, e.g. platinum [2].

2.1 Inconel 718

The particular superalloy chosen in this specific research programme is Inconel 718 or IN718 as it is usually called, which is widely used in gas turbine components such as stators, compressors and turbine discs. These components are comparatively large and subjected to high temperature. The stress/strain states in critical areas are often multiaxial, and it becomes important to know the constitutive as well as the fatigue damage evolution behaviour of the material under these conditions in order to predict a particular component's fatigue life.

IN718 is a Ni-Cr-Fe-Nb alloy with many good mechanical properties such as high yield and ultimate tensile strengths, good creep and rupture strengths, and high resistance to fatigue. IN718 contains large amounts of iron and such superalloys are sometimes referred to as nickel-iron superalloys. It is usually polycrystalline and like all modern superalloys it is precipitation hardened. As most superalloys containing large amounts of Fe it contains both coherent γ'' particles and γ' particles. The precipitates mainly contains niobium, aluminium and titanium [4]. The composition (in weight%) of IN718 is presented below.

Table 1: Composition of elements for IN718 [2]

Element	Weight%
Ni	balance
Cr	19.0
Mo	3.0
Nb	5.1
Al	0.5
Ti	0.9
Fe	18.5
C	0.04

2.1.1 Deformation mechanisms

Plastic deformation in a metallic material is dependent on movement of dislocations, where the latter are imperfections in the crystal structure. To inelastically deform a crystal with no defects demands very large stresses but to move a dislocation is much easier [5].

The deformation mechanisms of IN718 are different for different temperatures. At low temperature the deformation is dominated by twinning while for high temperatures it is dominated by slip [6].

In most materials plastic deformation occurs by slip on certain crystal planes, so-called slip planes. These dislocations move easily in these planes since they are close-packed with atoms and are relatively far from each other. Figure 2 show the crystal planes A and B. Slip is easiest achieved along the planes A as they are closely packed and have a larger separation.

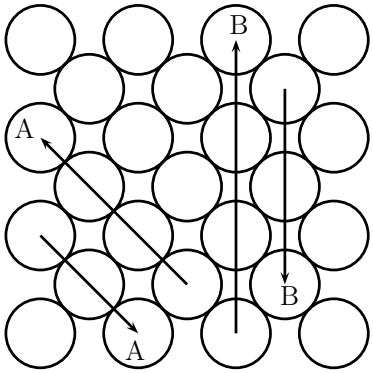

Figure 2: Slip

The dislocations in the slip planes move in certain directions called slip directions. These slip directions are also close-packed. The combination of a slip plane and a slip direction is called slip system. In the case of nickel with its FCC structure, the slip is along the close-packed {111} planes and the close-packed <110> directions [7], see Figure 3. In an FCC unit cell there is one atom in each corner as well as one atom centered on each face of the unit cell see Figure 4.

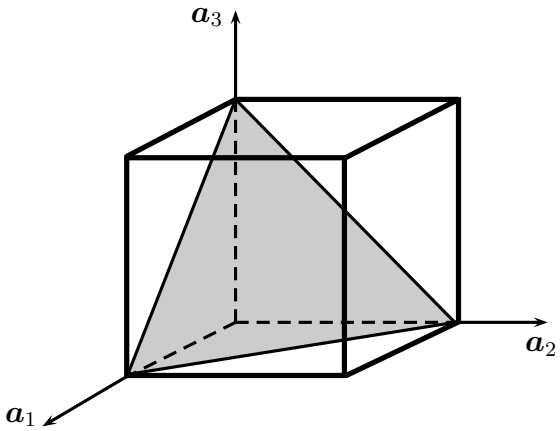

Figure 3: The (111) plane in the unit cell [8]

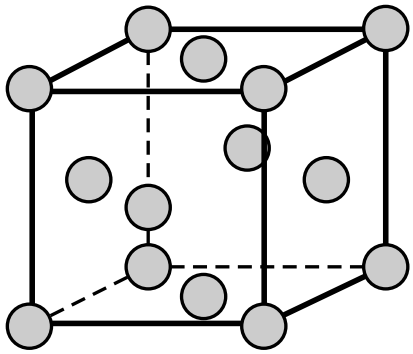

Figure 4: FCC crystal structure [8]

In case of twinning the deformation takes place in a thin so-called twin band, where the atoms are reordered to a mirror image of the surrounding structure [7], see Figure 5.

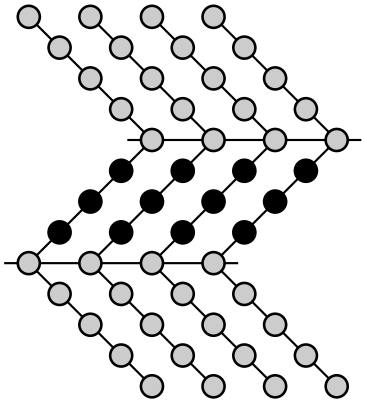

Figure 5: Twinning

2.1.2 Ordered structure, γ''

In IN718 the primary strengthening phase is not the γ' but instead a body-centered tetragonal (BCT) ordered structure called γ''. The γ' precipitates consists of Ni_3Al but the γ'' is instead usually made of Ni_3Nb.

The good high-temperature properties of IN718 are due to the coherency of the γ'' and the matrix and the small amount of slip systems for a body centered cubic (BCT) crystal [2]. Figure 6 shows a BCT crystal.

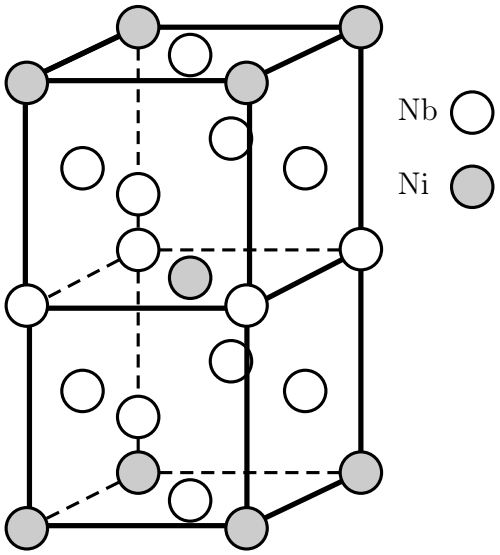

Figure 6: BCT crystal structure

2.1.3 Cyclic behaviour

In IN718 a rapid cyclic softening takes place during the initial cycling, which is followed by a stable cycling for most of the material life [6].

It is suggested that this softening is caused by formation of slip bands where elimination of the precipitates take place, leading to lower resistance of deformation. This elimination of precipitates is caused by a mechanism called particle cutting. In the normal case the desired effect of precipitation hardening is to hinder the movement of dislocations, but when the precipitates are too small the dislocations can cut through and split the precipitates. By this the precipitates loose their ability to hinder further dislocation movement. This mechanism is irreversible as the precipitates are permanently damaged [7].

Another mechanism leading to softening during cycling is dislocations escaping the pinning force by solute atoms. This effect is called dynamic strain aging. Usual phenomena attributed to dynamic strain aging are: yield stress plateaus as functions of temperature, upper yield points, reduced tensile elongation, negative strain rate sensitivity and serrated stress strain curves, see e.g. [9] & [10] for a discussion of the effect of such phenomena.

3 Theory

Some basic knowledge in continuum mechanics [11] and material mechanics [12] is needed for understanding the following sections. All relations are derived in a large deformation context and presented for Cartesian coordinates. Note: $\dot{x} = \frac{dx}{dt}$

3.1 Kinematics

In Figure 7, the local deformation of an elastoplastic body is shown from the *reference configuration* (Ω_0) to the *current configuration* (Ω). Instead of taking the direct way, with the use of the total deformation gradient $\boldsymbol{F}$, another way through the so called *isoclinic intermediate configuration* ($\bar{\Omega}_{iso}$) and the *intermediate configuration* ($\bar{\Omega}$) is taken, [13]. The first step consists of plastic deformation of the material (for an unchanged internal structure), described by the plastic deformation gradient $\boldsymbol{F}^p$. The material then undergoes a rotation $\boldsymbol{\phi}$. Finally, the material is both elastically stretched and rotated by the elastic deformation gradient $\boldsymbol{F}^e$ (an isothermal condition is assumed to prevail).

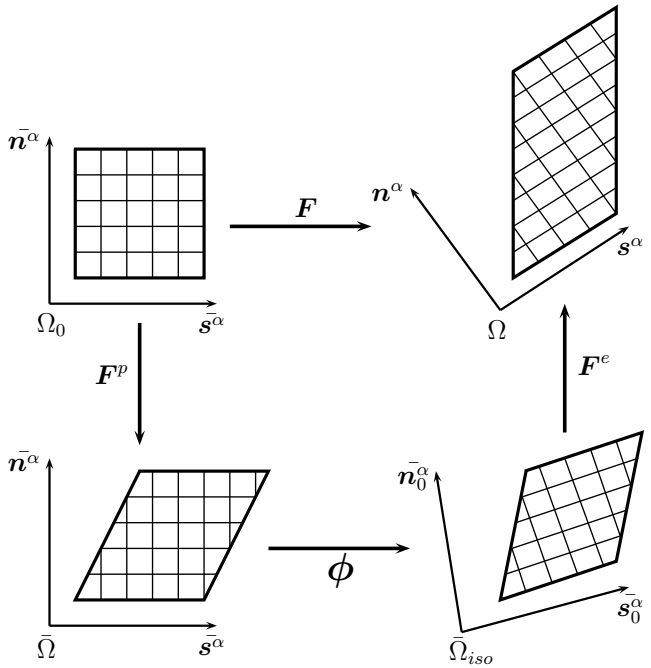

Figure 7: Kinematic description, with a rotation [8].

The total deformation gradient is thus split into an elastic part and a plastic part, by the following multiplicative decomposition

$$\boldsymbol{F} = \boldsymbol{F}^e \boldsymbol{\phi} \boldsymbol{F}^p \tag{1}$$

In the subsequent discussion the rotation $\boldsymbol{\phi}$ is set equal to the unit tensor, implying that the material exhibits no such rotation. Therefore, the material description in Figure 8 is used instead, where the isoclinic intermediate configuration becomes the intermediate configuration.

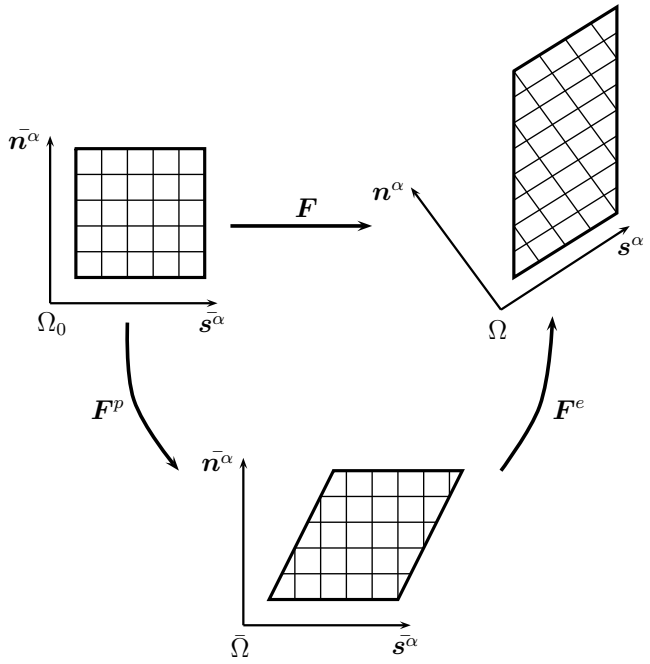

Figure 8: Kinematic description, without a rotation $\boldsymbol{\phi}$. [8]

The multiplicative decomposition is then expressed as [14]

$$\boldsymbol{F} = \boldsymbol{F}^e \boldsymbol{F}^p \tag{2}$$

The velocity gradient can then also be expressed in an elastic part and a plastic part.

$$\boldsymbol{L} = \dot{\boldsymbol{F}} \boldsymbol{F}^{-1} = \dot{\boldsymbol{F}}^e \boldsymbol{F}^{e^{-1}} + \boldsymbol{F}^e \dot{\boldsymbol{F}}^p \boldsymbol{F}^{p^{-1}} \boldsymbol{F}^{e^{-1}} \tag{3}$$

From Equation (3) the following can be defined

$$\boldsymbol{L}^e = \dot{\boldsymbol{F}}^e \boldsymbol{F}^{e^{-1}} \tag{4}$$

$$\boldsymbol{L}^p = \boldsymbol{F}^e \dot{\boldsymbol{F}}^p \boldsymbol{F}^{p^{-1}} \boldsymbol{F}^{e^{-1}} \tag{5}$$

$$\bar{\boldsymbol{L}}^p = \dot{\boldsymbol{F}}^p \boldsymbol{F}^{p^{-1}} \tag{6}$$

where $\boldsymbol{L}^e$, $\boldsymbol{L}^p$ are the elastic and plastic velocity gradient, respectively, defined in the current configuration (Ω) while $\bar{\boldsymbol{L}}^p$ is the plastic velocity gradient defined in the intermediate configuration ($\bar{\Omega}$).

The velocity gradient can be divided into one *symmetric* part and one *skew-symmetric* part.

$$\boldsymbol{L} = \frac{1}{2}\left(\boldsymbol{L} + \boldsymbol{L}^T\right) + \frac{1}{2}\left(\boldsymbol{L} - \boldsymbol{L}^T\right) = \boldsymbol{D} + \boldsymbol{W} \tag{7}$$

where $\boldsymbol{D}$ is the rate of deformation tensor (symmetric) and $\boldsymbol{W}$ is the spin tensor (skew-symmetric). These two can each be divided into an elastic part and a plastic part, accordingly to

$$\boldsymbol{D} = \boldsymbol{D}^e + \boldsymbol{D}^p \tag{8}$$

$$\boldsymbol{W} = \boldsymbol{W}^e + \boldsymbol{W}^p \tag{9}$$

where

$$\boldsymbol{D}^e = \frac{1}{2}\left(\boldsymbol{L}^e + \boldsymbol{L}^{e^T}\right),\ \boldsymbol{D}^p = \frac{1}{2}\left(\boldsymbol{L}^p + \boldsymbol{L}^{p^T}\right) \tag{10}$$

$$\boldsymbol{W}^e = \frac{1}{2}\left(\boldsymbol{L}^e - \boldsymbol{L}^{e^T}\right),\ \boldsymbol{W}^p = \frac{1}{2}\left(\boldsymbol{L}^p - \boldsymbol{L}^{p^T}\right) \tag{11}$$

The elastic Green-Lagrange strain tensor $\bar{\boldsymbol{E}}^e$ measured relative to the intermediate configuration is defined as

$$\bar{\boldsymbol{E}}^e = \frac{1}{2}\left(\boldsymbol{F}^{e^T}\boldsymbol{F}^e - \boldsymbol{I}\right) = \frac{1}{2}\left(\bar{\boldsymbol{C}}^e - \boldsymbol{I}\right) \tag{12}$$

where $\bar{\boldsymbol{C}}^e$ is the elastic right Cauchy-Green strain tensor relative to the intermediate configuration.

The relationship between the elastic rate of deformation tensor $\boldsymbol{D}^e$ defined in the current configuration and the elastic Green-Lagrange strain rate tensor $\dot{\bar{\boldsymbol{E}}}^e$ defined in the intermediate configuration is given by a *push-forward* or a *pull-back* operation [15]

$$\boldsymbol{D}^e = \boldsymbol{F}^{e^{-T}} \dot{\bar{\boldsymbol{E}}}^e \boldsymbol{F}^{e^{-1}},\ \dot{\bar{\boldsymbol{E}}}^e = \boldsymbol{F}^{e^T} \boldsymbol{D}^e \boldsymbol{F}^e \tag{13}$$

The 2:nd Piola-Kirchhoff stress tensor $\bar{\boldsymbol{S}}$ defined in the intermediate configuration can be expressed by a *pull-back* of the Kirchhoff stress tensor $\boldsymbol{\tau}$ from the current configuration by the following

$$\bar{\boldsymbol{S}} = \boldsymbol{F}^{e^{-1}}\boldsymbol{\tau}\boldsymbol{F}^{e^{-T}} \Rightarrow \boldsymbol{\tau} = \boldsymbol{F}^{e}\bar{\boldsymbol{S}}\boldsymbol{F}^{e^{T}} = \mathcal{J}\boldsymbol{\sigma} \tag{14}$$

where $\mathcal{J} = \det \boldsymbol{F}^e$. As can be seen, in order to receive the Cauchy stress tensor the Kirchhoff stress tensor is scaled by the Jacobian determinant [15].

The internal power $\mathcal{P}^{int}$, when a body is deformed, is defined as

$$\mathcal{P}^{int} = \int_{\Omega} \boldsymbol{\sigma} : \boldsymbol{D} dV \tag{15}$$

The internal power can be divided into an elastic part and a plastic part

$$\mathcal{P}^{int} = \int_{\Omega} \boldsymbol{\sigma} : \boldsymbol{D}^e dV + \int_{\Omega} \boldsymbol{\sigma} : \boldsymbol{D}^p dV \tag{16}$$

The elastic part is transformed by a regular pull-back operation to the intermediate configuration, accordingly to

$$\begin{aligned}
\int_{\Omega} \boldsymbol{\sigma} : \boldsymbol{D}^e dV &= \int_{\Omega} \frac{1}{\mathcal{J}}\boldsymbol{\tau} : \boldsymbol{D}^e dV = \int_{\bar{\Omega}} \boldsymbol{\tau} : \boldsymbol{D}^e d\bar{V} = \\
&= \int_{\bar{\Omega}} (\boldsymbol{F}^e \bar{\boldsymbol{S}} \boldsymbol{F}^{e^T}) : (\boldsymbol{F}^{e^{-T}} \dot{\boldsymbol{E}}^e \boldsymbol{F}^{e^{-1}}) d\bar{V} = \\
&= \int_{\bar{\Omega}} tr(\boldsymbol{F}^e \bar{\boldsymbol{S}}^T \underbrace{\boldsymbol{F}^{e^T}\boldsymbol{F}^{e^{-T}}}_{\boldsymbol{I}} \dot{\boldsymbol{E}}^e \boldsymbol{F}^{e^{-1}}) d\bar{V} = \\
&= \int_{\bar{\Omega}} tr(\underbrace{\boldsymbol{F}^{e^{-1}}\boldsymbol{F}^e}_{\boldsymbol{I}} \bar{\boldsymbol{S}}^T \dot{\bar{\boldsymbol{E}}}^e) d\bar{V} = \int_{\bar{\Omega}} \bar{\boldsymbol{S}} : \dot{\bar{\boldsymbol{E}}}^e d\bar{V}
\end{aligned} \tag{17}$$

while we from the plastic part, due to the symmetry of $\boldsymbol{\sigma}$ get

$$\begin{aligned}
\int_{\Omega} \boldsymbol{\sigma} : \boldsymbol{D}^p dV &= \int_{\Omega} \frac{1}{\mathcal{J}}\boldsymbol{\tau} : \boldsymbol{D}^p dV = \int_{\bar{\Omega}} \boldsymbol{\tau} : \boldsymbol{D}^p d\bar{V} \overset{\text{sym}}{=} \int_{\bar{\Omega}} \boldsymbol{\tau} : \boldsymbol{L}^p d\bar{V} = \\
= \int_{\bar{\Omega}} (\boldsymbol{F}^e \bar{\boldsymbol{S}} \boldsymbol{F}^{e^T}) : (\boldsymbol{F}^e \bar{\boldsymbol{L}}^p \boldsymbol{F}^{e^{-1}}) d\bar{V} &= \int_{\bar{\Omega}} tr(\boldsymbol{F}^e \bar{\boldsymbol{S}}^T \underbrace{\boldsymbol{F}^{e^T}\boldsymbol{F}^e}_{\bar{\boldsymbol{C}}^e} \bar{\boldsymbol{L}}^p \boldsymbol{F}^{e^{-1}}) d\bar{V} = \\
&= \int_{\bar{\Omega}} tr(\underbrace{\boldsymbol{F}^{e^{-1}}\boldsymbol{F}^e}_{\boldsymbol{I}} \bar{\boldsymbol{S}}^T \bar{\boldsymbol{C}}^e \bar{\boldsymbol{L}}^p) d\bar{V} = \int_{\bar{\Omega}} \bar{\boldsymbol{C}}^{e^T} \bar{\boldsymbol{S}} : \bar{\boldsymbol{L}}^p d\bar{V} = \\
&= \int_{\bar{\Omega}} \bar{\boldsymbol{C}}^e \bar{\boldsymbol{S}} : \bar{\boldsymbol{L}}^p d\bar{V} = \int_{\bar{\Omega}} \boldsymbol{\varpi} : \bar{\boldsymbol{L}}^p d\bar{V}
\end{aligned} \tag{18}$$

where $\boldsymbol{\mathcal{M}}$ is the Mandel stress tensor. The Mandel stress tensor is a *non-symmetric* tensor and it is defined in the intermediate configuration. From Equation (18) it can be seen that the Mandel stress tensor in relation to the 2:nd Piola-Kirchhoff stress tensor is given by

$$\boldsymbol{\mathcal{M}} = \bar{\boldsymbol{C}}^e \bar{\boldsymbol{S}} \tag{19}$$

This can be further developed with the insertion of Equation (14), so that it relates to the Kirchhoff stress tensor by

$$\boldsymbol{\mathcal{M}} = \boldsymbol{F}^{e^T} \boldsymbol{\tau} \boldsymbol{F}^{e^{-T}} \tag{20}$$

It is to be noted that for small elastic strains, for which $\bar{\boldsymbol{C}}^e \approx \boldsymbol{I}$, it follows that $\boldsymbol{\mathcal{M}} \approx \bar{\boldsymbol{S}}$ where $\bar{\boldsymbol{S}}$ is symmetric. Since this is the prevailing situation in gas turbine applications we will in what follows assume that $\boldsymbol{\mathcal{M}}$ may be replaced by $\bar{\boldsymbol{S}}$.

3.2 Thermodynamics

The internal energy is assumed given by

$$e = e(\bar{\boldsymbol{E}}^e, \boldsymbol{b}) \tag{21}$$

where $\bar{\boldsymbol{E}}^e$ is the elastic Green-Lagrange strain tensor in the intermediate configuration while $\boldsymbol{b}$ is an internal state variable, which accounts for the loading history of the material. Differentiating this yields

$$\dot{e} = \frac{\partial e}{\partial \bar{\boldsymbol{E}}^e} : \dot{\bar{\boldsymbol{E}}}^e + \frac{\partial e}{\partial \boldsymbol{b}} : \dot{\boldsymbol{b}} \tag{22}$$

A combination of the 1:st and 2:nd principles of thermodynamics for the case of isothermal conditions gives the so called Clausius-Duhem inequality [16]

$$\boldsymbol{\sigma} : \boldsymbol{D} - \rho \dot{e} \geq 0 \tag{23}$$

where ρ is the density in the current configuration, or by $\rho_0 = \mathcal{J}\rho$ the following inequality is received

$$\boldsymbol{\tau} : \boldsymbol{D} - \rho_0 \dot{e} \geq 0 \tag{24}$$

Equation (24) can be further developed with the insertion of Equation (22) and by separating e and $\boldsymbol{D}$ into their elastic and plastic parts, for $\boldsymbol{D}$ from Equations (17) and (18), respectively. This gives

$$\bar{\boldsymbol{S}} : \dot{\bar{\boldsymbol{E}}}^e + \boldsymbol{\mathfrak{m}} : \bar{\boldsymbol{L}}^p - \rho_0(\dot{e}_{el} + \dot{e}_{pl}) \geq 0 \tag{25}$$

where

$$\dot{e}_{el} = \frac{\partial e}{\partial \bar{\boldsymbol{E}}^e} : \dot{\bar{\boldsymbol{E}}}^e \tag{26}$$

and

$$\dot{e}_{pl} = \frac{\partial e}{\partial \boldsymbol{b}} : \dot{\boldsymbol{b}} \tag{27}$$

e_{el} is the elastic part of the internal energy and e_{pl} is the plastic part of the internal energy.

Considering only elastic deformations and noting that the Clausius-Duhem inequality holds for any particular $\dot{\bar{\boldsymbol{E}}}^e$ it follows that

$$\bar{\boldsymbol{S}} = \rho_0 \frac{\partial e}{\partial \bar{\boldsymbol{E}}^e} \tag{28}$$

Furthermore, by assuming that this equation of state also is valid for inelastic processes, we get the following reduced dissipation inequality.

$$\mathcal{D} = \boldsymbol{\mathcal{M}} : \bar{\boldsymbol{L}}^p - \rho_0 \dot{e}_{pl} \geq 0 \tag{29}$$

4 Adopted constitutive description

To capture the cyclic behavior of IN718 a constitutive model with a backstress evolution of Armstrong-Frederick type can be used [12]. This is a non-linear kinematic hardening model with a backstress including two parts, a hardening part and a relaxation part. In the adopted model the plastic flow is described by a viscous law.

4.1 Basic elastoplastic description

The plastic velocity gradient defined in the intermediate configuration is assumed to obey the following viscoplastic relation [17]

$$\bar{\boldsymbol{L}}^p = \dot{\lambda}\frac{\partial f}{\partial \boldsymbol{\mathcal{M}}} \tag{30}$$

where

$$\dot{\lambda} = \lambda_0 \left(\frac{\sigma_e}{\sigma_Y}\right)^m \tag{31}$$

and

$$\frac{\partial f}{\partial \boldsymbol{\mathcal{M}}} = \frac{3(\mathrm{dev}\boldsymbol{\mathcal{M}} - \mathrm{dev}\boldsymbol{B})}{2\sigma_e} \tag{32}$$

where σ_e is the effective stress according to von Mises, σ_Y is the yield limit, $\dot{\lambda}$ is the plastic multiplier, $\boldsymbol{B}$ is the backstress (explained later), dev$\boldsymbol{\mathcal{M}}$ is the deviatoric part of the Mandel stress tensor, dev$\boldsymbol{B}$ is the deviatoric part of the backstress tensor and λ_0 and m are positive constants.

As can be seen since $\boldsymbol{\mathcal{M}} \approx \bar{\boldsymbol{S}}$, and thus $\boldsymbol{\mathcal{M}}$ is symmetric, it follows that $\bar{\boldsymbol{L}}^p$ is symmetric and thus close to $\bar{\boldsymbol{D}}^p$.

4.2 Hardening description

In the adopted model the hardening description is based on a backstress formulation. The evolution of the backstress tensor is of Armstrong-Frederick type [12]. To address the kinematic hardening the second order tensor $\boldsymbol{b}$ is used according to $e_{pl} = e_{pl}(\boldsymbol{b})$.

By this it follows that

$$\mathcal{D} = \boldsymbol{\sigma}:\bar{\boldsymbol{L}}^p - \boldsymbol{B}:\dot{\boldsymbol{b}} \geq 0 \tag{33}$$

where

$$\boldsymbol{B} = \rho_0 \frac{de_{pl}}{d\boldsymbol{b}} \tag{34}$$

specifically it will be assumed that

$$\rho_0 e_{pl} = \frac{C_1}{2}\boldsymbol{b}:\boldsymbol{b} \tag{35}$$

implying

$$\boldsymbol{B} = C_1\boldsymbol{b} \tag{36}$$

and that

$$\dot{\boldsymbol{b}} = \boldsymbol{D}^p - C_2\boldsymbol{B} \mid \boldsymbol{D}^p \mid \tag{37}$$

$\boldsymbol{B}$ is referred to as the backstress, C_1 and C_2 are positive material constants, $\boldsymbol{D}^p$ is the plastic rate of deformation tensor and $\mid \boldsymbol{D}^p \mid = (\boldsymbol{D}^p:\boldsymbol{D}^p)^{1/2}$ [18].

In Eq. 37, describing the backstress the two terms can be physically motivated from the microstructural effects they are to describe [3]. The first term describes hardening due to pile up of dislocations against obstacles such as solute atoms, precipitates and grain boundaries, and is to be proportional to the rate of plastic deformation. The second term represents dynamic recovery, i.e. the reduction of dislocation density and stored energy that occurs simultaneously with deformation. This is e.g. due to annihilation of dislocations of opposite sign. The recovery term is proportional to both the rate of plastic deformation and to the current backstress as these two variables imply more interacting dislocations. A problem with the Armstrong-Frederick nonlinear kinematic hardening based rule is that it always leads to a shakedown to a zero value mean stress. However, the predicted shake-down is usually much too fast compared to experimental results [19].

4.3 Thermodynamics

To verify the thermodynamic validity of the above-specified model a control of the reduced dissipation inequality is needed.

From Eq. (33) giving the dissipation inequality for the model we get

$$\begin{aligned}\mathcal{D} = \boldsymbol{\mathfrak{m}}{:}\bar{\boldsymbol{L}}^p - \boldsymbol{B}{:}\dot{\boldsymbol{b}} = \boldsymbol{\mathfrak{m}}{:}\bar{\boldsymbol{L}}^p - \boldsymbol{B}{:}\boldsymbol{D}^p + C_2\boldsymbol{B}{:}\boldsymbol{B} \mid \boldsymbol{D}^p \mid = \\ = (\boldsymbol{\mathfrak{m}} - \boldsymbol{B}){:}\bar{\boldsymbol{L}}^p + C_2\boldsymbol{B}{:}\boldsymbol{B} \mid \boldsymbol{D}^p \mid = \\ = (\boldsymbol{\mathfrak{m}} - \boldsymbol{B}){:}\dot{\lambda}\frac{3(\mathrm{dev}\boldsymbol{\mathfrak{m}} - \mathrm{dev}\boldsymbol{B})}{2\sigma_e} + C_2\boldsymbol{B}{:}\boldsymbol{B} \mid \boldsymbol{D}^p \mid = \\ = \dot{\lambda}\frac{3}{2}(\mathrm{dev}\boldsymbol{\mathfrak{m}} - \mathrm{dev}\boldsymbol{B}){:}(\mathrm{dev}\boldsymbol{\mathfrak{m}} - \mathrm{dev}\boldsymbol{B})\frac{1}{\sigma_e} + C_2\boldsymbol{B}{:}\boldsymbol{B} \mid \boldsymbol{D}^p \mid = \\ = \sigma_e\dot{\lambda} + C_2\boldsymbol{B}{:}\boldsymbol{B} \mid \boldsymbol{D}^p \mid \geq 0\end{aligned} \tag{38}$$

where $\boldsymbol{B}{:}\boldsymbol{D}^p = \boldsymbol{B}{:}\boldsymbol{L}^p$ hence $\boldsymbol{B}{:}\boldsymbol{W}^p = 0$, $\boldsymbol{D}^p$ and $\boldsymbol{B}$ are symmetric.

Thus, since

$$\dot{\lambda} \geq 0 \tag{39}$$

$$\sigma_e \geq 0 \tag{40}$$

$$C_2\boldsymbol{B}{:}\boldsymbol{B} \mid \boldsymbol{D}^p \mid \geq 0 \tag{41}$$

this implies that the 2:nd principle of thermodynamics is fulfilled.

5 Implementation

5.1 Numerical treatment

Based on the discussion in previous chapters, a material model was constructed for the FEM program LS-DYNA [20]. The model was written in the programming language FORTRAN77. The basics of the written material model is that the total deformation gradient is calculated by the FEM program and the material model calculates the Cauchy stress tensor $\boldsymbol{\sigma}$, plastic deformation gradient tensor $\boldsymbol{F}^P$ and the backstress tensor $\boldsymbol{B}$ for the next time step (n+1).

5.1.1 Specific operations

The FEM program delivers the total deformation gradient, and by using this and the plastic deformation gradient for the previous time step (n), a trial value of the elastic deformation gradient is calculated.

$$\boldsymbol{F}^e_{trial} = \boldsymbol{F}_{n+1}\boldsymbol{F}_n^{p^{-1}} \tag{42}$$

Trial values of the elastic Green-Lagrange strain tensor defined in the intermediate configuration, the 2:nd Piola-Kirchhoff stress tensor defined in the intermediate configuration and the Mandel stress tensor is calculated (observe that the subscript (n+1) is skipped in association with the trial state).

$$\bar{\boldsymbol{E}}^e_{trial} = \frac{1}{2}(\boldsymbol{F}^{e^T}_{trial}\boldsymbol{F}^e_{trial} - \boldsymbol{I}) \tag{43}$$

$$\bar{\boldsymbol{S}}^e_{trial} = C_l\bar{\boldsymbol{E}}^e_{trial} \tag{44}$$

$$\boldsymbol{\mathcal{M}}_{trial} = \boldsymbol{F}^{e^T}_{trial}\boldsymbol{F}^e_{trial}\bar{\boldsymbol{S}}^e_{trial} \tag{45}$$

where C_l is the elastic tangent stiffness tensor.

Using this and the viscoplastic relation presented in Eq. 30 and the backstress tensor from the previous time step, the plastic velocity gradient defined in the intermediate configuration is calculated.

$$\bar{\boldsymbol{L}}^p_{trial} = \dot{\lambda}\left.\frac{\partial f}{\partial \boldsymbol{\mathcal{M}}}\right|_{trial} = \lambda_0\left(\frac{\sigma_{e_{trial}}}{\sigma_Y}\right)^m \frac{3(\mathrm{dev}\boldsymbol{\mathcal{M}}_{trial} - \mathrm{dev}\boldsymbol{B}_n)}{2\sigma_{e_{trial}}} \tag{46}$$

where the effective stress is calculated as

$$\sigma_{e_{trial}} = \sqrt{\frac{3}{2}(\mathrm{dev}\boldsymbol{\varpi}_{trial} - \mathrm{dev}\boldsymbol{B}_n) : (\mathrm{dev}\boldsymbol{\varpi}_{trial} - \mathrm{dev}\boldsymbol{B}_n)} \tag{47}$$

Using the previously calculated plastic velocity gradient and the plastic deformation gradient from the previous time step, the plastic deformation gradient for the current time step can be calculated using an Euler forward scheme, according to.

$$\bar{\boldsymbol{L}}^p_{trial} = \dot{\boldsymbol{F}}^p_{trial}\boldsymbol{F}^{p^{-1}}_n = \left(\frac{\boldsymbol{F}^p_{n+1} - \boldsymbol{F}^p_n}{\Delta t}\right)\boldsymbol{F}^{p^{-1}}_n \tag{48}$$

which gives

$$\boldsymbol{F}^p_{n+1} = (\boldsymbol{I} + \Delta t\bar{\boldsymbol{L}}^p_{n+1})\boldsymbol{F}^p_n \tag{49}$$

Using the calculated plastic deformation gradient and the deformation gradient delivered from the FEM program, the elastic deformation gradient for the current time step can be calculated.

$$\boldsymbol{F}^e_{n+1} = \boldsymbol{F}_{n+1}\boldsymbol{F}^{p^{-1}}_{n+1} \tag{50}$$

Using these values, the elastic Green-Lagrange strain tensor defined in the intermediate configuration and the 2:nd Piola-Kirchhoff stress tensor defined in the intermediate configuration, both for the current time step, is calculated.

$$\bar{\boldsymbol{E}}^e_{n+1} = \frac{1}{2}(\boldsymbol{F}^{e^T}_{n+1}\boldsymbol{F}^e_{n+1} - \boldsymbol{I}) \tag{51}$$

$$\bar{\boldsymbol{S}}^e_{n+1} = C_l\bar{\boldsymbol{E}}^e_{n+1} \tag{52}$$

The Cauchy stress tensor is calculated and delivered to the FEM program according to

$$\boldsymbol{\sigma}_{n+1} = \frac{1}{det\boldsymbol{F}^e_{n+1}}\boldsymbol{F}^e_{n+1}\bar{\boldsymbol{S}}_{n+1}\boldsymbol{F}^{eT}_{n+1} \tag{53}$$

The backstress must then be updated for the next timestep. The backstress tensor for the time step (n+1) depends on the inner state variable, which is calculated using the backstress from the previous timestep (n) by an Euler forward scheme.

$$\boldsymbol{B}_{n+1} = \boldsymbol{b}_{n+1} C_1 \tag{54}$$

$$\boldsymbol{b}_{n+1} = \boldsymbol{b}_n + \bar{\boldsymbol{D}}^p \Delta t - C_2 \sqrt{\bar{\boldsymbol{D}}^p : \bar{\boldsymbol{D}}^p}\, \boldsymbol{B}_n \Delta t \tag{55}$$

where the rate of plastic deformation tensor defined in the intermediate configuration is calculated as $\bar{\boldsymbol{D}}^p = \frac{1}{2}(\bar{\boldsymbol{L}}^p + \bar{\boldsymbol{L}}^{p^T})$.

Finally the plastic deformation gradient and the backstress are saved to history variables to be used in the next time step.

5.2 LS-DYNA input

Nine parameters are needed as input data for LS-DYNA, and these are presented in the table below.

Table 2: Material parameters

$\mathrm{cm}(1) = K$	Bulk modulus
$\mathrm{cm}(2) = G$	Shear modulus
$\mathrm{cm}(3) = E$	Youngs modulus
$\mathrm{cm}(4) = \nu$	Poisson's ratio
$\mathrm{cm}(5) = \lambda_0$	Material constant
$\mathrm{cm}(6) = m$	Material constant
$\mathrm{cm}(7) = \sigma_Y$	Yield limit
$\mathrm{cm}(8) = C_1$	Material constant
$\mathrm{cm}(9) = C_2$	Material constant

The first two, the bulk modulus and the shear modulus are only needed in LS-DYNA for calculating an estimate of the critical time step (needed for explicit analysis), but are otherwise not used in the material model. The density is also set in the input file but not used by the material model.

5.3 Verification

To verify the implemented material model a cube with side length 1 m was constructed. The cube was meshed with one brick element with one integration point. The cube was uniaxially given a cyclic strain (ϵ) and then a stress-strain curve was plotted. Two different load cases were used:

$$R_\epsilon = \frac{\epsilon_{min}}{\epsilon_{max}} = 0 \tag{56}$$

and

$$R_\epsilon = \frac{\epsilon_{min}}{\epsilon_{max}} = -1 \tag{57}$$

R_ϵ is called the strain ratio.

The material parameters used in the simulations are presented in Table 3, where E, ν and σ_Y are relevant for IN718 and the rest is selected without any validation.

Table 3: Material parameters for the simulations

E	ν	λ_0	m	σ_Y	C_1	C_2
199 GPa	0.3	0.01	20	1250 MPa	$1.0 \cdot 10^{10}$	$7.0 \cdot 10^9$

In case of R=0, the first positive loading ends in a larger stress state than the following positive loading. The stress is said to have shakendown. In this type of loading, a rapid shakedown to mid stress equal to zero is expected during the first few load cycles, the larger the inelastic deformation is the more rapid is the shakedown [12]. As expected it can be seen in Figure 10, that there is a shakedown to approximately zero mean stress.

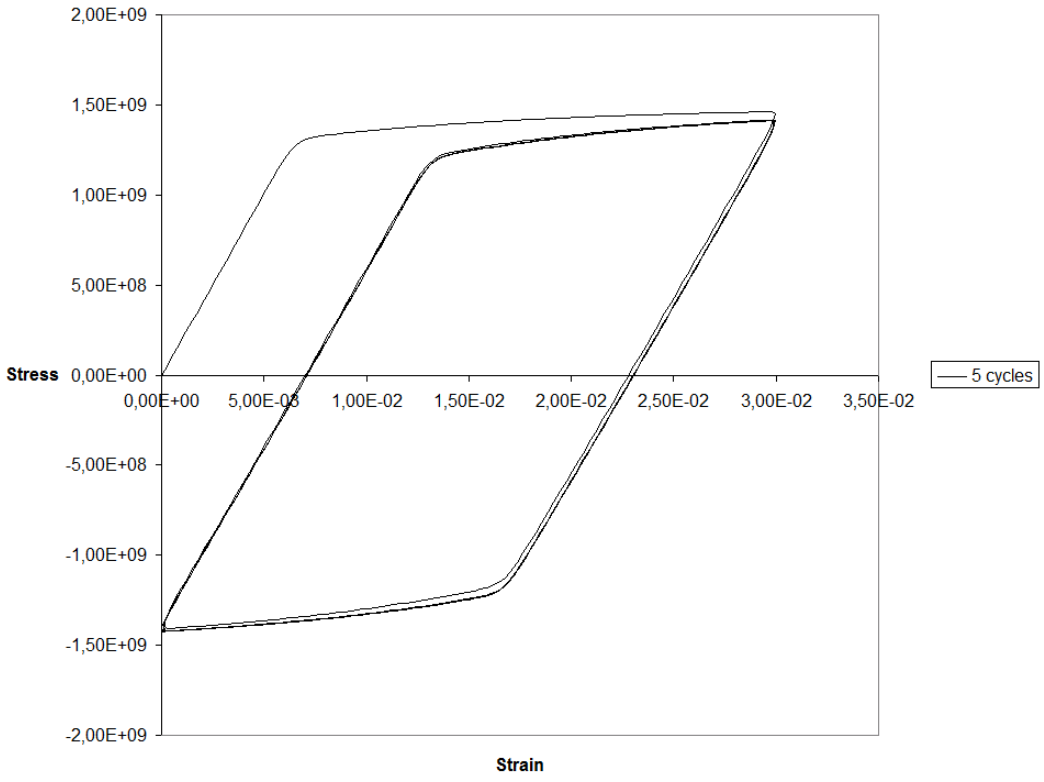

Figure 9: Five load cycles for $R_\epsilon = 0$

The cycles stabilize, as can be seen in Figure 9 where the first and 5:th cycle are approximately the same.

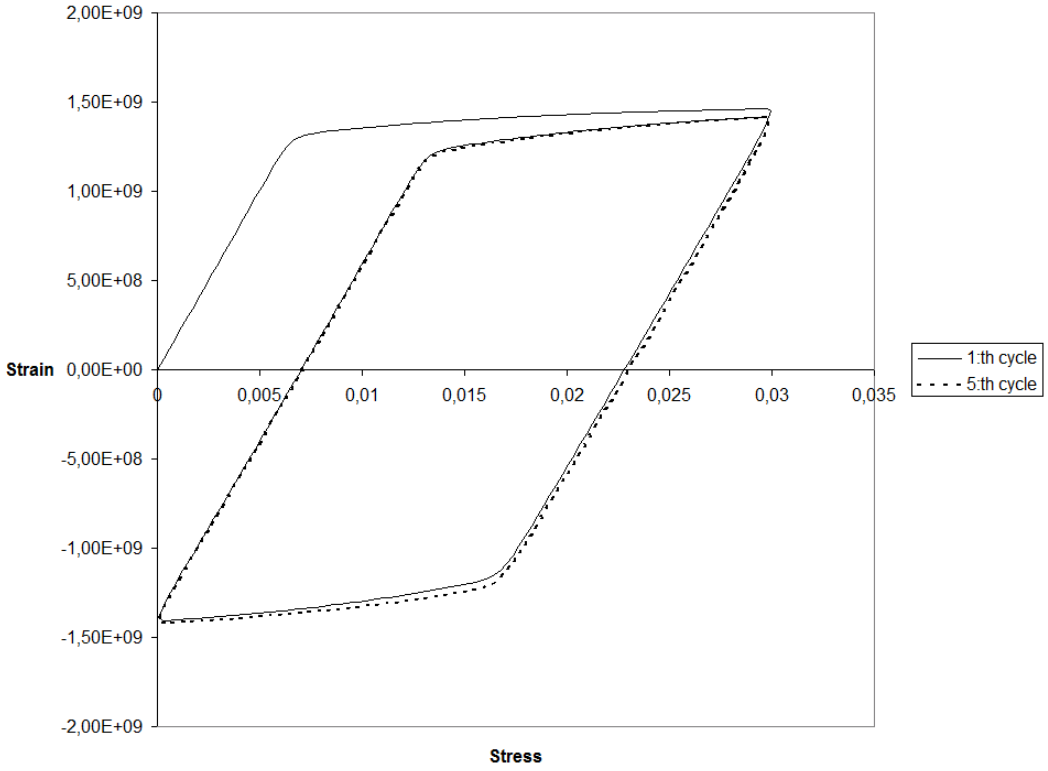

Figure 10: First and 5th load cycle for $R_\epsilon = 0$

In the case of R=-1 a stable load cycle is received from the first cycle, see Figure 11, which is also as expected, se e.g. [12].

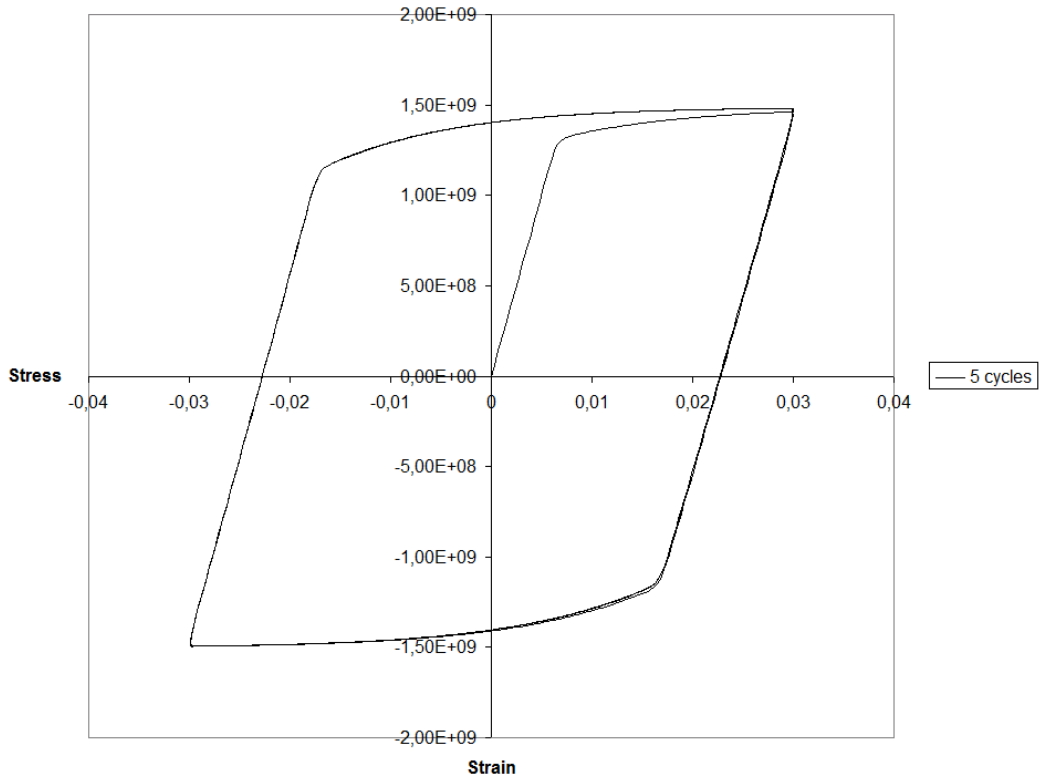

Figure 11: Five load cycles for $R_\epsilon = -1$

6 Conclusions, discussion and suggestions for further work

6.1 Conclusions and discussion

As a summary of the work presented in this report, here follow some conclusions and discussions:

- It is of importance to have a physically well motivated constitutive model. As is presented in the report, nickel-base superalloys are very complex an have got a lot of specific behaviours. This implies that a good knowledge in material science is necessary.
- The modelling work was done in several steps starting from writing a simple elastic material model, later moving on to introduce plasticity and hardening. Models should initially be kept simple and expanded only when physically motivated. A too general and complex model often means that it is computationally ineffective and hard to calibrate.
- The presented model can be used to simulate cyclic behaviour of the nickel-base superalloy IN718, but there is still a lot of physical phenomena which have to be addressed i.e. cyclic softening (see below).
- Work on addressing strain-rate independent plasticity and cyclic softening has started but is not presented in this report.

6.2 Future work

To finalize a constitutive modell for IN718 further issues have to be addressed:

- IN718 exhibits a rapid cyclic softening. This cyclic softening essentially influences the inelastic strain range and thus affects the fatigue life. Thus, cyclic softening has to be implemented into the constitutive model.
- In gas turbines the material experiences very high temperatures and is an important source of fatigue. Temperature dependence is therefore necessary to implement.
- Another problem is to address the fact that in the industry there is not enough time to compute every cycle in a simulation of perhaps several

hundreds of cycles. This means it is important to do some kind of jump from virgin material data to midlife material data.

- For low temperatures the material does not exhibit any strain rate dependence, which must be addressed in a future constitutive model.

References

[1] Stekovic S., 2007, *Low Cylce Fatigue and Thermo-Mechanical Fatigue of Uncoated and Coated Nickel-base Superalloys*, Linköping University, Linköping Studies in Science and Technology Dissertation No. 1129.

[2] Reed R.C., 2006, *The Superalloys - Fundamentals and Applications*, Cambridge University Press, Cambridge.

[3] Almroth P., 2003, *Constitutive modeling of a nickel base superalloy - with a focus on gas turbine applications*, Linköping University, Linköping Studies in Science and Technology Dissertation No. 1014.

[4] Korth G.E., 1991, *Effects of various parameters on the fatigue life of alloy 718*, The Minerals, Metals & Material Society.

[5] Askeland D.R., 2001, *The Science and Engineering of Material*, Nelson Thornes Ltd, Cheltenham.

[6] Almroth P., 2003, *TMF-LCF life modelling of material 638103, IN718*, Siemens Industrial Turbomachinery, Technical report RT GRC 219/06.

[7] Hertzberg R.W., 1996, *Deformation and Fracture Mechanics of Engineering Materials*, John Wiley & Sons Inc.

[8] Leidermark D., 2008, *Mechanical Behaviour of Single-Crystal Nickel-base Superalloys*, Linköping University, Linköping, Mater thesis LIU-IEI-TEK-A–08/00283–SE.

[9] Hale, Weaver, 2001, *Activation energy calculations for discontinuos yielding in Inconel 718SPF*, Material sience, v300, p. 153-164.

[10] Weaver, Hale, 2001, *Effects of precipitation on serrated yielding in Inconel 718*, Superalloys 718, 625, 706 and Various Derivatives, TMS.

[11] Mase G. T., Mase G. E., 1999, *Continuum Mechanics for Engineers*, CRC Press LLC, Boca Raton.

[12] Ottosen S. N., Ristinma M., 2005, *The Mechanics of Constitutive Modeling*, Elsavier, Oxford.

[13] Haupt P., 2002, *Continuum Mechanics and Theory of Materials*, Springer-Verlag, Berlin Heidelberg.

[14] Khan A.S., Huang S., 1995, *Continuum Theory of Plasticity*, John Wiley & Sons Inc, New York.

[15] Belytschko T., Liu W.K., Moran B., 2000, *Nonlinear Finite Elements for Continua and Structures*, John Wiley & Sons Ltd, Chichester.

[16] Lemaitre J., Chaboche J.-L., 1990, *Mechanics of Solid Materials*, Cambridge University Press, Avon.

[17] Kalidindi S.R., 1992, *Polycrystal Plasticity: Constitutive Modeling and Deformation Processing*, Massachusetts Institute of Technology, Cambridge.

[18] Holzapfel G.A., 2000, *Continuum Mechanics for Engineers*, John Wiley & Sons Ltd, Chichester.

[19] Chaboche J.L., 2008, *A review of some plasticity and viscoplasticity constitutive theories*, International Journal of Plasticity, 24, p. 1642-1693.

[20] LS-DYNA, 2008-01-25, http://www.ls-dyna.com/